2,6-Diaryl-9,10-anthraquinones as models for electron-accepting polymers†

Julien E. Gautrot,*[a] Philip Hodge,*[a] Domenico Cupertino[b] and Madeleine Helliwell[a]

Received (in Montpellier, France) 29th January 2007, Accepted 9th May 2007
First published as an Advance Article on the web 6th June 2007
DOI: 10.1039/b701257h

Anthraquinone derivatives have been little used in microelectronics though they are attractive scaffolds due to their electron-accepting properties. As part of a preliminary study, a series of conjugated anthraquinone derivatives has been synthesised. The crystal structures of 2,6-diphenyl-9,10-anthraquinone, 2,6-di(thien-2′-yl)-9,10-anthraquinone and 2,6-bis(9′,9′-dioctylfluoren-2′-yl)-9,10-anthraquinone are presented. The UV-Vis absorption spectra of the anthraquinone derivatives synthesised are characterised in each case by the presence of a very intense long-wavelength band that we attribute to intramolecular charge transfer (CT) from the electron-rich aromatic substituents to the electron-deficient anthraquinone moiety. The fluorescence of these compounds is also strongly affected by this intramolecular CT and quantum yields up to 6.8×10^{-2} were found in solution. This long wavelength emission in the yellow-orange region is reminiscent of the fluorescence of fluorenone derivatives substituted with aromatic groups, including fluorenone-containing polyfluorenes. The relatively high electron affinity of these compounds together with their tunable emission suggests their potential application in organic electronics. Additionally, the electrochemical behaviour of the present compounds reveals a partial destabilisation of both of the aromatic rings in the anthraquinone moiety. Finally, chemical doping experiments were conducted. These clearly show the extended conjugation characteristic of the reduced states of anthraquinone.

Introduction

The field of organic molecules for electronics is growing rapidly. Organic materials are now used in a wide range of applications such as organic light emitting diodes (OLEDs),[1,2] field-effect transistors (OFETs),[3–5] photovoltaics,[6] sensors[7] and smart windows.[8] The vast majority of the materials that have been developed so far display low electron affinities (EAs). However, high EA materials are still required in order to improve the performance of devices and industry is very keen on developing this area.

Examples of low-molecular-weight organic materials with significant EAs that have been developed so far include tetracyanoquinodimethane,[9] oligothiophenes end-capped with perfluoroarenes,[10] perfluoropentacene,[11] quinoxalines[12] and naphthalenecarboxylic diimide (NTCDI) derivatives.[13] The few examples of high EA polymeric materials are based on oxobenzimidazoquinolines,[14] quinoxalines,[15,16] thiazoles[17] and oxadiazoles.[18] However, other properties of these various materials are not always ideal for applications in electronic devices. Stability is obviously an issue, but other properties such as charge carrier mobilities or fluorescence quantum yields also need to be improved. Moreover, although great progress has been made concerning the increase of EA itself, materials displaying EA of around 3.5 eV are still scarce. Examples include oxobenzimidazoquinolines[5] and NTCDI derivatives.[13] Materials displaying such high EA have been predicted to show improved stability in FETs for example.[19]

A family of electron-accepting molecules that has received very little attention in connection with electronic devices, despite their important role for electron transport in photosynthesis,[20] is the quinone family. Amongst this family 9,10-anthraquinone (**1**) displays both significant EA and good thermal and electrochemical stability. Moreover, derivatives of this molecule are synthetically relatively easily accessible. Yamamoto and co-workers showed that it is possible to polymerise dichloro-9,10-anthraquinone derivatives using nickel-based catalysts,[21,22] while research conducted within our group showed that it is possible to synthesise poly(9,10-anthraquinone-2,6-diyl) *via* a precursor route.[23] It was found that 9,10-anthraquinone-based polymers display very poor solubility in common organic solvents unless the anthraquinone moiety is incorporated into the polymer backbone *via* 1,4-linkages. More recently, we found that coupling of 1,4-dibromo-9,10-anthraquinones or the bistriflate of 1,4-dihydroxy-9,10-anthraquinone *via* Yamamoto and Suzuki couplings afforded polymeric materials.[24] However, molecules synthesised possessing a 1,4-linkage display high torsion angles and low backbone π-conjugation.[24] This led us to

[a] *Department of Chemistry, University of Manchester, Oxford Road, Manchester, UK M13 9PL. E-mail: juliengautrot@yahoo.fr;Philip.Hodge@man.ac.uk*
[b] *Avecia, Blackley, Manchester, UK*

† Electronic supplementary information (ESI) available: UV-Vis spectra of **3a–e** in various solvents, cyclic voltammograms of compounds **1** and **3a,c–e**. See DOI: 10.1039/b701257h

consider polymers containing anthraquinone units coupled *via* the 2- and 6-positions. Due to the very poor solubility of poly(anthraquinone-2,6-diyl) itself,[23] polymers of the type AA–BB are needed where AA represents the anthraquinone-containing unit and BB is a solubilising and possibly ordering unit. Prior to synthesising such polymers it was considered of interest to prepare and study some simple model compounds.

In this article, the synthesis of a series of 2,6-diaryl-9,10-anthraquinones, **3a–e**, is described as well as the spectroscopic and electrochemical properties of these materials. Certain 2,6-diaryl-9,10-anthraquinones were found to display surprisingly high fluorescence quantum yields due to effective intramolecular charge transfer (CT), which is reminiscent of the photophysical processes encountered in 2,7-diaryl-9-fluorenone and fluorenone-containing polyfluorenes. Moreover their electrochemical behaviour and X-ray crystal structure provide evidence of a decrease in the aromatic character of the anthraquinone benzene rings. Finally, the structure of the reduced species, and especially the way the negative charges are delocalised, were probed by UV-Vis spectroscopy of the chemically reduced molecules.

Experimental

General methods

Organic solutions were dried over magnesium sulfate. For purifications with flash column chromatography Merck 9385 silica gel 60 (230–400 mesh) was used. Thin layer chromatography (TLC) was carried out using Merck silica gel (60–254 mesh) coated on PET plates. All chemicals and solvents were purchased from Aldrich, Lancaster, Fluka, Avocado or Strem. They were used without further purification unless stated. $Pd(PPh_3)_4$[25] and the pinacol ester of 9,9-dioctylfluorene-2-boronic acid[26] were synthesised as described in the literature.

Melting points were measured using a Gallenkamp melting point apparatus. FT-IR spectra were recorded on a Perkin Elmer spectrometer equipped with a He/Ne 633 nm (<0.4 mW) laser. UV-Vis spectra were recorded using a Unicam UV 300 spectrometer. Fluorescence spectra were measured using a Perkin Elmer LS 55 spectrometer. Fluorescence quantum yields were measured using quinine sulfate in aqueous H_2SO_4 solutions for the calibration.[27] NMR spectra were recorded on a Varian Inova 300 MHz spectrometer. For labelling of protons, the IUPAC nomenclature is used. Mass spectrometry was carried out using a Micromass Trio 2000 instrument for EI/CI mass spectra (MS), a Micromass platform instrument for electrospray MS and a Micromass TOF Spec 2E instrument for MALDI TOF MS. Elemental analysis was performed by the Microanalysis laboratory of the Department of Chemistry, University of Manchester. DSC measurements were carried out on a SEIKO Instruments DSC 220G instrument. TGA measurements were made on a Seiko Instruments TG/DTA 220 instrument. Cyclic voltammograms (CVs) were recorded using a CH Instruments Electrochemical Workstation. The working electrode was glassy carbon, the counter electrode was a platinum wire and the reference electrode was Ag/AgCl. All CV measurements were carried out under an argon atmosphere. Abbreviations used to describe various spectra and data: s, singlet; d, doublet; t, triplet; q, quadruplet; m, multiplet; bp, broad peak; bd, broad doublet; bm, broad multiplet; obs, observed; req, required; sh, shoulder.

Chemical doping experiments

In a typical experiment a solution of 9,10-anthraquinone (**1**) (4.6×10^{-5} mol L^{-1}) in *N*-methylpyrrolidinone (NMP) (UV-Vis spectroscopy grade) and a reductant solution of sodium hydrosulfite (4.6×10^{-3} mol L^{-1}) and sodium hydroxide (4.6×10^{-2} mol L^{-1}) in deionised water were degassed by gently bubbling argon through for 20 min. The quinone solution (2.00 mL) was syringed into a spectroscopic cell (1 cm Spectrosil cell) fitted with a septum and further degassed for 5 min. A first UV-Vis spectrum was recorded at this stage. The reductant solution (0.05 mL) was then added to the spectroscopic cell and the resulting mixture quickly shaken. Two further UV-Vis spectra were recorded just after addition of the reductant and after allowing the mixture to rest for 10 min. Finally, some reductant solution (0.05 mL) was added to the spectroscopic cell, the mixture shaken and a final UV-Vis spectrum recorded. The reference was an NMP solution in a matched cell. Identical amounts of reductant were added to the reference each time.

Syntheses

Bistriflate of 2,6-dihydroxy-9,10-anthraquinone (2). 2,6-Dihydroxyanthraquinone (5.00 g, 20.8 mmol) was placed in a flame-dried round-bottomed flask (1-neck, 100 mL), fitted with a septum, under nitrogen. Dry pyridine (30 mL) and triflic anhydride (13.1 g, 46.2 mmol) were added *via* the septum while cooling the reaction mixture with an ice bath. The resulting mixture was stirred for 12 h at room temperature. The mixture was then poured into aqueous hydrochloric acid (0.1 M, 400 mL) and extracted with dichloromethane (3 × 30 mL). The organic phase was extracted with aqueous hydrochloric acid (0.1 M, 2 × 50 mL) and water (3 × 50 mL), dried, filtered and the solvent evaporated off under vacuum to afford an orange solid. Recrystallisation from isopropanol and toluene afforded beige needles which were sublimed (120 °C, 0.1 mbar) to afford a pale yellow powder (7.61 g, 73%). Mp 219–221 °C; IR (NaCl, cm^{-1}) 1671, 1593, 1426, 1322, 1300, 1249, 1209, 1136, 897, 864, 832, 769 and 749; ^1H NMR ($CDCl_3$, ppm) δ 8.48 (2H; d, J = 9 Hz; H-4), 8.21 (2H; d, J = 3 Hz; H-1) and 7.74 (2H; q, J = 3 and 8.6 Hz; H-3); ^{13}C NMR ($CDCl_3$, ppm) δ 120.6, 127.6, 131.0, 132.9, 135.7, 153.9 and 180.1; MS (MALDI) 506 g mol^{-1}, $C_{16}H_6O_8F_6S_2H^+$ requires 506 g mol^{-1}.

General procedure for the synthesis of 2,6-diaryl-9,10-anthraquinones. 2,6-Diphenyl-9,10-anthraquinone (3a). The bistriflate of 2,6-dihydroxy-9,10-anthraquinone (**2**) (250 mg, 0.58 mmol), phenylboronic acid (177 mg, 1.45 mmol) and palladium[0]-tetrakis(triphenylphosphine) (65 mg, 58 μmol) were placed in a round-bottomed flask (3-neck, 100 mL), fitted with a condenser, under nitrogen. Tetrahydrofuran (20 mL, degassed with argon) and aqueous sodium carbonate (1.0 M, 5 mL, degassed with argon) were added *via* a septum. The mixture was heated under reflux overnight then poured onto aqueous hydrochloric acid (0.1 M, 200 mL). The aqueous phase was extracted with

dichloromethane (2 × 50 mL), the extracts washed with water (3 × 50 mL), dried and the solvent evaporated under vacuum. This afforded a brown solid (227 mg). Sublimation (120 °C, 0.1 mbar) afforded yellow crystals (186 mg, 89%). Mp 265–266 °C (lit,[28] 265 °C); IR (NaCl, cm^{-1}) 1671, 1592, 1447, 1311, 1279, 1161, 951, 911, 856 and 733; ^1H NMR ($CDCl_3$, ppm) δ 8.55 (2H; d, J = 2 Hz; H-1), 8.39 (2H; d, J = 8 Hz; H-4), 8.02 (2H; dd, J = 2 and 8 Hz; H-3), 7.74 (4H; m) and 7.57–7.42 (6H; bm); ^{13}C NMR ($CDCl_3$, ppm) δ 125.8, 127.6, 128.2, 128.3, 128.4, 129.4, 132.5, 132.6, 139.2, 147.2 and 183.2; MS (MALDI) 362 g mol^{-1}, $C_{26}H_{16}O_2H^+$ requires 361 g mol^{-1}; UV-Vis spectrum (chloroform, nm) λ_{max} (ε) 283 (49,500), 309 (27,900) and 355 (13,200).

2,6-Di(thien-2′-yl)-9,10-anthraquinone (3b). Following the above procedure bistriflate **2** (1.00 g, 2.31 mmol) was reacted with thiophen-2-boronic acid (652 mg, 5.09 mmol) and palladium[0]tetrakis(triphenylphosphine) (110 mg, 95 μmol). This gave compound **3b** (528 mg, 61%). Mp 228–229 °C (lit,[28] 228 °C); IR (KBr, cm^{-1}) 1668, 1590, 1424, 1357, 1313, 1214, 1165, 905, 824, 741 and 711; ^1H NMR ($CDCl_3$, ppm) δ 8.53 (2H; d, J = 2 Hz; H-1), 8.33 (2H; d, J = 8 Hz; H-4), 8.01 (2H; dd, J = 2 and 8 Hz; H-3), 7.60 (2H; dd, J = 1 and 4 Hz; H-3′), 7.46 (2H; dd, J = 1 and 5 Hz; H-4′) and 7.18 (2H; dd, J = 4 and 5 Hz; H-5′); ^{13}C NMR ($CDCl_3$, ppm) δ 124.1, 125.9, 127.8, 128.6, 128.9, 130.8, 132.2, 134.5, 140.4, 142.4 and 182.7; MS (MALDI) 373 g mol^{-1}, $C_{22}H_{12}O_2S_2H^+$ requires 373 g mol^{-1}; microanalysis: calc: C, 70.9%, H, 3.2%, S, 17.2%; found: C, 70.7%, H, 2.7%, S, 16.8%; UV-Vis spectrum (chloroform, nm) λ_{max} (ε) 301 (34,300), 340 (37,500) and 384 (19,500).

2,6-Bis(9′,9′-dioctylfluoren-2′-yl)-9,10-anthraquinone (3c). Following the above procedure bistriflate **2** (159 mg, 0.37 mmol) was reacted with the pinacol ester of 9,9-dioctylfluorene-2-boronic acid (400 mg, 0.77 mmol) and palladium[0] tetrakis(triphenylphosphine) (44 mg, 38 μmol). This gave compound **3c** (291 mg, 80%). Mp (DSC) 160 °C; IR (NaCl, cm^{-1}) 2927, 2855, 1673, 1592, 1466, 1312, 1291, 967, 831 and 746; ^1H NMR ($CDCl_3$, ppm) δ 8.66 (2H; d, J = 2 Hz; H-1), 8.45 (2H; d, J = 8 Hz; H-4), 8.12 (2H; dd, J = 2 and 8 Hz; H-3), 7.84 (2H; d, J = 8 Hz), 7.80–7.70 (6H; m), 7.42–7.33 (6H; m), 2.05 (8H; dd, J = 5 and 11 Hz; H-1″), 1.29–0.98 (40H; m), 0.80 (12H; t, J = 7 Hz; H-8″) and 0.68 (8H; bm; H-2″); ^{13}C NMR ($CDCl_3$, ppm) δ 14.3, 22.9, 24.1, 29.5, 30.3, 32.0, 40.7, 55.6, 120.4, 120.6, 121.8, 123.3, 125.7, 126.6, 127.2, 127.9, 128.4, 132.3, 132.6, 134.4, 137.9, 140.6, 142.4, 147.8, 151.5, 152.2 and 183.5; microanalysis: calc: C, 87.7%, H, 9.0%; found: C, 87.5%, H, 9.4%; MS (MALDI) 985 g mol^{-1}, $C_{72}H_{88}O_2H^+$ requires 986 g mol^{-1}; UV-Vis spectrum (chloroform, nm) λ_{max} (ε) 315 (53,600), 338 (38,200; sh) and 398 (23,500).

2,6-Bis(4′-hexylthien-2′-yl)-9,10-anthraquinone (3d). Following the above procedure bistriflate **2** (500 mg, 1.16 mmol) was reacted with the pinacol ester of 4-hexylthiophene-2-boronic acid (850 mg, 2.90 mmol) and palladium[0]tetrakis(triphenylphosphine) (110 mg, 95 μmol). This gave compound **3d** (437 mg, 70%). Mp (DSC) 164 °C; IR (NaCl, cm^{-1}) 2930, 2852, 1669, 1592, 1440, 1315, 1296, 1210, 945, 908, 836, 746 and 708; ^1H NMR ($CDCl_3$, ppm) δ 8.48 (2H; d, J = 2 Hz; H-1), 8.30 (2H; d, J = 8 Hz; H-4), 7.95 (2H; q, J = 2 and 8 Hz; H-3), 7.43 (2H; d, J = 1 Hz; H-3′), 7.03 (2H; d, J = 1 Hz; H-5′), 2.66 (4H; t, J = 7 Hz; H-1″), 1.67 (4H; m; H-2″), 1.45–1.24 (12H; m) and 0.92 (6H; t, J = 7 Hz; H-6″); ^{13}C NMR ($CDCl_3$, ppm) δ 14.4, 22.9, 29.2, 30.7, 30.8, 31.9, 122.6, 123.7, 127.3, 128.5, 130.4, 132.0, 134.4, 140.6, 141.9, 145.3 and 182.7; MS (MALDI) 545 g mol^{-1}, $C_{34}H_{46}O_2S_2H^+$ requires 542 g mol^{-1}; microanalysis: calc: C, 75.5%, H, 6.7%, S, 11.9%; found: C, 74.0%, H, 6.7%, S, 11.0%; UV-Vis spectrum (chloroform, nm) λ_{max} (ε) 305 (29,500), 347 (30,300) and 396 (18,100).

2,6-Di(furan-2′-yl)-9,10-anthraquinone (3e). Following the above procedure bistriflate **2** (250 mg, 0.58 mmol) was reacted with furan-2-boronic ester (193 mg, 1.74 mmol) and palladium[0]tetrakis(triphenylphosphine) (65 mg, 58 μmol). This gave compound **3e** (171 mg, 87%). TGA: T_{dec}, 278 °C; IR (NaCl, cm^{-1}) 1670, 1597, 1494, 1460, 1310, 1275, 1022, 966, 907, 884, 800 and 744; ^1H NMR ($CDCl_3$ and d-TFA, ppm) δ 8.51 (2H; d, J = 2 Hz; H-1), 8.31 (2H; d, J = 8 Hz; H-4), 8.09 (2H; dd, J = 2 and 8 Hz; H-3), 7.60 (2H; d, J = 2 Hz; H3′), 7.04 (2H; d, J = 4 Hz; H5′) and 6.58 (2H; dd, J = 4 and 2 Hz; H-4′); ^{13}C NMR ($CDCl_3$ and d-TFA, ppm) δ 108.7, 110.3, 112.5, 129.2, 129.3, 131.3, 134.3, 137.7, 144.9, 151.7 and 185.1; MS (MALDI) 342 g mol^{-1}, $C_{22}H_{12}O_4H^+$ requires 341 g mol^{-1}; microanalysis: calc: C, 77.7%, H, 3.6%; found: C, 76.8%, H, 3.3%; UV-Vis spectrum (chloroform, nm) λ_{max} (ε) 304 (22,200), 338 (15,500) and 397 (6,800).

Pinacol ester of 4-hexylthiophene-2-boronic acid (5). 3-Hexylthiophene (3.05 g, 18.1 mmol) and tetrahydrofuran (50 mL, anhydrous) were placed in a flame-dried round-bottomed flask (1-neck, 100 mL) fitted with a septum, under nitrogen. The mixture was cooled down to −78 °C and stirred at this temperature for five min. Butyl lithium (8.0 mL, 20 mmol) was added dropwise, using a syringe, and the mixture was stirred at −78 °C for 2 h. 2-Isopropoxy-4,4,5,5-tetramethyl-1,3,2-dioxaborolane (11.1 mL, 54.1 mmol) was finally added quickly and the mixture was left to heat up to room temperature and stirred for 12 h. The solvent was then evaporated off under vacuum to afford a colourless oil which was dissolved in dichloromethane (50 mL), washed with aqueous hydrochloric acid (0.1 M, 2 × 30 mL), water (3 × 50 mL), dried over magnesium sulfate, filtered off and the solvent evaporated under vacuum. Chromatography (silica, petroleum ether/ethyl acetate 90/10) afforded the desired product as a colourless oil (3.76 g, 71%). IR (NaCl, cm^{-1}) 2974, 2929, 2857, 1545, 1445, 1380, 1326, 1270, 1214, 1144, 1027, 961, 854, 772 and 685; ^1H NMR ($CDCl_3$) δ 7.47 (1H; d, J 1 Hz; H-5), 7.21 (1H; d, J 1 Hz; H-3), 2.63 (2H; t, J = 7 Hz; H-1′), 1.60 (2H; m; H-2′), 1.34 (12H; s; Me), 1.29 (6H; m), 0.89 (3H; t, J = 7 Hz; H-6′); ^{13}C NMR ($CDCl_3$) δ 15.3, 22.7, 24.5, 30.4, 31.1, 33.7, 35.2, 83.9, 128.4, 138.8, 138.9 and 146.1 ppm; MS (EI/CI) 294 g mol^{-1}, $C_{16}H_{27}BO_2SH^+$ requires 295 g mol^{-1}.

X-Ray crystallography

Single crystals suitable for X-ray crystallography of **3a**, **3b** and **3c** were obtained from toluene, mounted in inert oil and transferred to the cold gas stream of the diffractometer.

Table 1 Selected crystallographic data for compounds **3a–c**

3a		**3b**		**3c**	
C–C bond	Length (in Å)	C–C bond	Length (in Å)	C–C bond	Length (in Å)
C4–C8	1.4870 (16)	C4–C5	1.459 (3)	C6–C8	1.483 (3)
C4–C5	1.4008 (17)	C5–C10	1.404 (3)	C5–C6	1.399 (3)
C3–C4	1.4001 (16)	C5–C6	1.399 (3)	C6–C7	1.393 (3)
C5–C6	1.3852 (17)	C9–C10	1.375 (3)	C4–C5	1.377 (3)
C2–C3	1.3916 (16)	C6–C7	1.389 (3)	C1A–C7	1.392 (3)
C6–C7	1.3947 (16)	C8–C9	1.395 (3)	C3–C4	1.396 (3)
C2–C7	1.4042 (16)	C7–C8	1.401 (3)	C1A–C3	1.394 (3)
C1A–C7	1.4882 (16)	C8–C11A	1.478 (3)	C2–C3	1.483 (3)

The crystallographer's nomenclature (see Fig. 2) was used for numbering of the atoms.

Crystal data for 3a. $C_{26}H_{16}O_2$, M = 360.39, monoclinic, a = 23.3924(17), b = 9.5829(7), c = 19.3455(14) Å, β = 126.6490(10)°, U = 3479.3(4) Å^3, T = 100 K, space group $C2/c$ (no. 15), Z = 8, μ(Mo-Kα) = 0.086 mm^{-1}, 13 478 reflections measured, 3567 unique (R_{int} = 0.055) which were used in all calculations. The asymmetric unit contains two crystallographically independent half molecules, with the full molecules being generated by inversion The final $R(F)$ = 0.0356 using 2918 with $I > 2\sigma(I)$, wR_2 = 0.944 (all data). See Fig. 2a and Table 1. CCDC reference number 646790.‡

Crystal data for 3b. $C_{22}H_{12}O_2S_2$, M = 372.44, monoclinic, a = 5.6860(15), b = 10.210(3), c = 14.072(4)) Å, α = 97.506(4), β = 92.789(4), γ = 90.580(4)°, U = 808.8(4) Å^3, T = 100 K, space group $P\bar{1}$ (no. 2), Z = 2, μ(Mo-Kα) = 0.344 mm^{-1}, 6461 reflections measured, 3252 unique (R_{int} = 0.043) which were used in all calculations. The asymmetric unit contains two crystallographically independent half molecules, with the full molecules being generated by inversion. See Fig. 2b and Table 1. The S1 and S2 atoms are disordered with C3 and C14, respectively, and occupancies of the disordered components were constrained to sum to unity with the main fraction for molecule 1 having a final occupancy of 0.878(2) and for molecule 2, 0.573(3). Restraints on the geometry and the atomic displacement parameters in the regions of disorder were applied. Some of the disordered atoms were refined isotropically, whilst all other non hydrogen atoms were refined anisotropically. The final $R(F)$ was 0.0428 using 2373 with $I > 2\sigma(I)$, wR_2 = 0.1085 (all data). CCDC reference number 646791.‡

Crystal data for 3c. $C_{72}H_{88}O_2$, M = 372.44, monoclinic, a = 8.736(6), b = 8.973(6), c = 18.358(12) Å, α = 89.562(13) β = 88.762(12) γ = 81.196(12)°, U = 1421.7(17) Å^3, T = 100 K, space group $P\bar{1}/n$ (no. 2), Z = 1, μ(Mo-Kα) = 0.067 mm^{-1}, 10 213 reflections measured, 4984 unique (R_{int} = 0.064) which were used in all calculations. The asymmetric unit contains half the molecule with the other half generated by inversion. See Fig. 2c and Table 1. The atoms C34–C36 are disordered over 2 sites, each at an occupancy of 0.5, and restraints were used in their geometry. Non-H atoms were refined anisotropically, except for the disordered C atoms. The final $R(F)$ was 0.0557 using 2815 with $I > 2\sigma(I)$, wR_2 = 0.1263 (all data). CCDC reference number 646792.‡

‡ CCDC reference numbers 646790–646792. For crystallographic data in CIF or other electronic format see DOI: 10.1039/b701257h

Results and discussion

Syntheses

An attractive approach to the synthesis of 2,6-diaryl-9,10-anthraquinones is the Suzuki coupling of either 2,6-dibromo-9,10-anthraquinone or the bistriflate of 2,6-dihydroxy-9,10-anthraquinone (**2**) with arylboronic acids or esters, as described in the literature for the synthesis of 2,6-dipyridyl-, 2,6-diphenyl- (**3a**) as well as 2,6-dithienyl-9,10-anthraquinone (**3b**).[28] Since the bistriflate **2** is very easily prepared from commercially available 2,6-dihydroxy-9,10-anthraquinone, this approach was used in the present work. The appropriate boronic acid or ester was chosen depending on commercial availability. The syntheses are summarised in Scheme 1. Purification of the products was achieved by chromatography, recrystallisation, sublimation or a combination of these techniques. The desired 2,6-diaryl-9,10-anthraquinones were obtained in yields higher than 60%.

Structural characterisation

The IR spectra clearly show bands typical of the anthraquinone moiety, especially the carbonyl stretching band near 1670 cm^{-1}. Other distinctive features such as aliphatic C–H stretching bands are observed where expected from the structure. The ^{1}H NMR spectra of all models display a set of anthraquinoid peaks that can be assigned to protons in the 1-, 3- and 4- positions (for an example see Fig. 1): a doublet for two protons near 8.5 ppm (H-1), a doublet for two protons near 8.3 ppm (H-4) and a quartet for two protons near 8.0 ppm (H-3). The peaks corresponding to the protons of the different aromatic moieties can be found at higer chemical field, consistent with the structures of the molecules. The ^{13}C NMR spectra of the different compounds show *one* single peak between 182 and 185 ppm, corresponding to the carbonyl carbons, consistent with the symmetry of the molecules.

X-ray crystal structures were obtained for models **3a**, **3b** and **3c** (see Fig. 2 and Table 1). These reveal interesting structural information (Fig. 2). First, the anthraquinone moiety is fully planar. This may seem obvious, but it is not the case for 1,4-diaryl substituted anthraquinones, due to the steric crowding of the aromatic substituents and the carbonyl oxygen.[25] Second, the dihedral angles between the least squares planes of the aromatic substituent and the anthraquinone moiety are quite small, especially when compared with those reported for

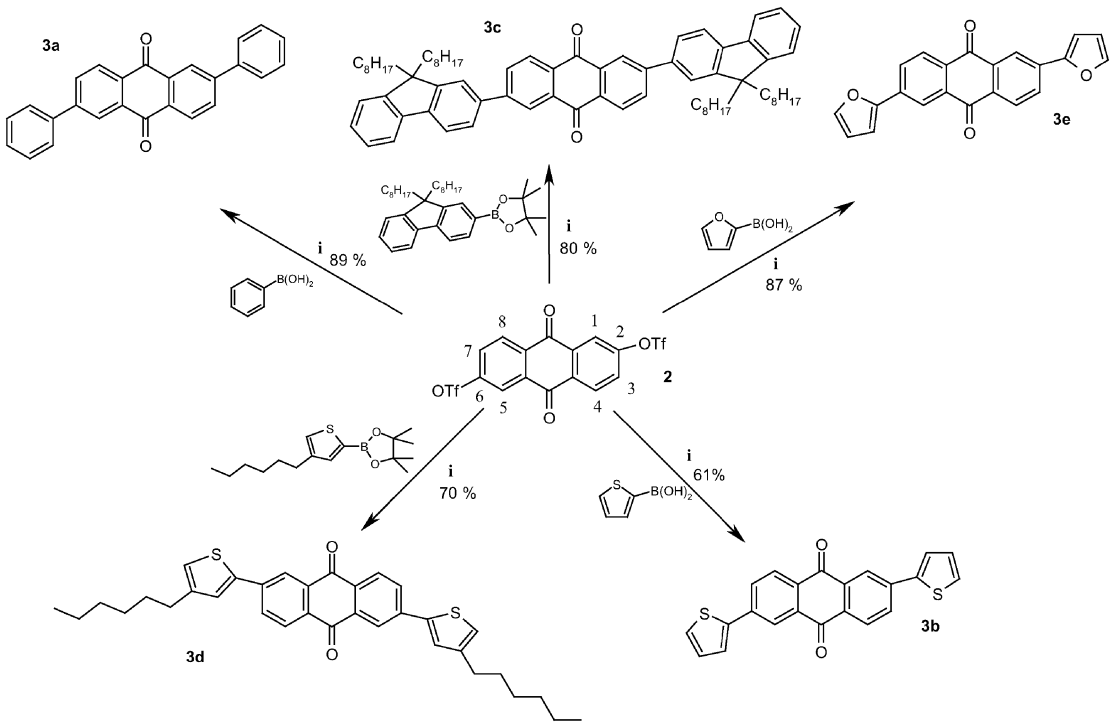

Scheme 1 Synthesis of 2,6-bisaryl-9,10-anthraquinones **3a–e**. i, $Pd(PPh_3)_4$, tetrahydrofuran, Na_2CO_3 (1.0 M). IUPAC nomenclature is indicated for **2**.

1,4-diaryl substituted anthraquinones which are in the region of 60–70°.[24] They are 30.15 and 33.25° for the two rotamers in the crystal, molecules 1 and 2, of **3a**, respectively, 6.71 and 17.16° for the two rotamers in the crystal, molecules 1 and 2, of **3b**, respectively and 31.11° for **3c**. Third, the C–C bond lengths between the aromatic substituent and the anthraquinone moiety are 1.487(2) and 1.485(2) Å for molecules 1 and 2 of **3a**, respectively, 1.459(3) and 1.458(3) Å for molecules 1 and 2 of **3b**, respectively and 1.483(3) Å, for **3c**. The correlation of this bond length with the nature of the aromatic substituent follows the same trend as the dihedral angles between the least squares planes. This phenomenon implies an increase of the double bond nature of this bond for **3b** compared with **3a** and **3c**. Finally, the substituted benzene rings, within the anthraquinone moiety, are found to have C–C bonds of different lengths. The C5–C6, C9–C10 and C4–C5 bonds (the nomenclature used here is that of the crystallographer, see Fig. 2) in **3a**, **3b** and **3c**, respectively are especially short (1.385(2) and 1.384(2) Å for molecules 1 and 2 of **3a**, respectively, 1.377(3) Å for **3c** and 1.375(3) and 1.378(3) Å for molecules 1 and 2 of **3b**, respectively) compared to the other bond length within the benzene ring (Table 1). Such differences in the bond length of a benzene ring are not usually encountered in fully aromatic benzene rings. Although the bond lengths of the different C–C bonds of the aromatic ring of anthraquinone (**1**) and other substituted derivatives are not equal (only benzene and other benzene derivatives belonging to C_6 or C_3 groups can have identical C–C bond lengths), the C1–C2 and C3–C4 bonds (here the IUPAC systematic nomenclature is used for the purpose of generality) of anthraquinone derivatives where no strong mesomeric effects take place are generally of equal lengths, as it is the case with 1,4-substituted anthraquinones.[24] Therefore, the X-ray data obtained for **3a–c** suggest a relative loss of aromaticity for the two benzene rings of the anthraquinone moiety due to an increase of the contribution of mesomers such as **4** (see Scheme 2). Such an aromatic destabilisation seems to increase with decreasing ionisation potential of the substituent (or rather that of the corresponding hydrogen-capped aromatic system, but we will refer to it as the ionisation potential of the substituent in the rest of the manuscript, for clarity) and the torsion angle and, as discussed below, will have important repercussions on the electrochemical behaviour of the different compounds.

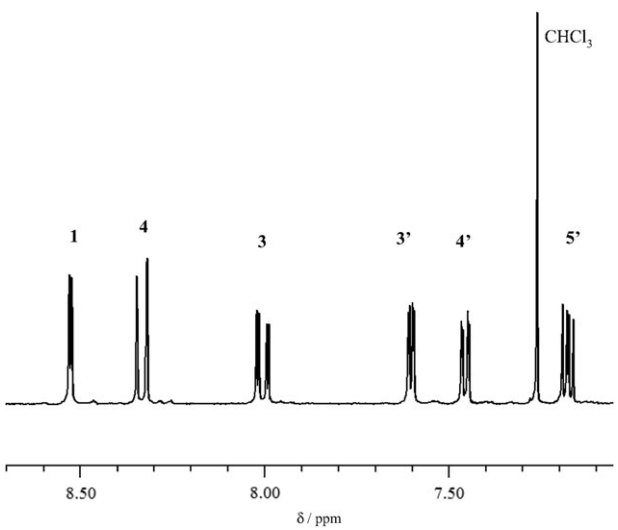

Fig. 1 ^{1}H NMR spectrum of compound **3b** in $CDCl_3$.

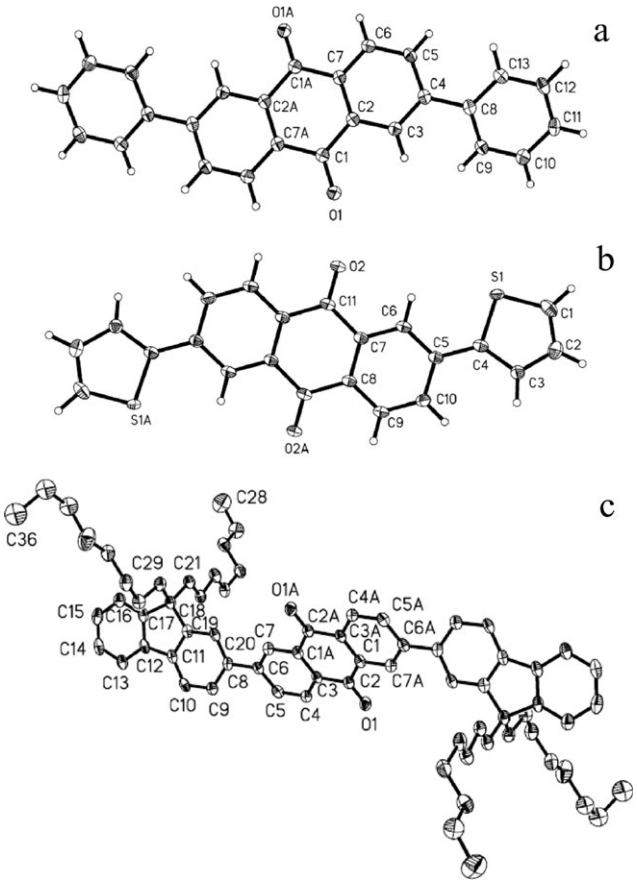

Fig. 2 Ortep plots of (a) **3a** [one of the crystallographically non-equivalent molecules (rotamers) present in the crystals of **3a**, with disordered atoms of the lower fraction component omitted for clarity], (b) **3b** [one of the crystallographically non-equivalent molecules (rotamers) present in the crystals of **3b**] and (c) **3c** (with one component of the disordered atoms omitted for clarity) with displacement ellipsoids drawn at the 50% probability level; the "A" letters in the atom labels indicate that these atoms are at equivalent position ($-x$, $1-y$, $2-z$) for Fig. 2a and 2c, and ($1-x$, $-y$, $2-z$) for Fig. 2b.

UV-Vis spectroscopy

The UV-Vis spectroscopy of anthraquinone and its derivatives has been the subject of many papers and reviews.[29–31] The results presented in this work were compared to this pool of data. The UV-Vis spectrum of anthraquinone itself displays four transitions above 240 nm.[29,31] The highest transition, near 400 nm, with a very weak extinction coefficient (typically less than 100 mol L^{-1} cm^{-1}) and vibrational features, has an n–π* nature. The three more intense bands near 250, 270 and 320 nm are π–π* transitions and possess, respectively benzenoid, quinonoid and benzenoid characters.[30]

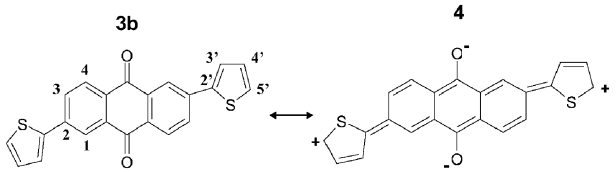

Scheme 2 Mesomer forms of **3b**.

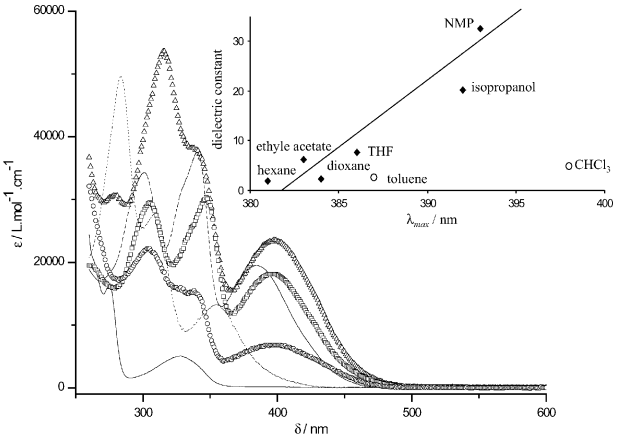

Fig. 3 UV-Vis spectra of 9,10-anthraquinone (**1**) (solid line), compounds **3a** (dotted line); **3b** (dashed line), **3c** (triangles), **3d** (squares) and **3e** (circles) in chloroform. Inset, plot of the λ_{max} of absorption for the highest transition *versus* the dielectric constant of the solvent in the case of compound **3c**.

The UV-Vis spectra obtained for **1** and models **3a–e** share similar features (Fig. 3). The main difference is the highest transition: the UV-Vis spectra of models **3a–e** all display an intense ($\varepsilon > 10\,000$ mol L^{-1} cm^{-1}) transition above 350 nm. This transition is too intense to have an n–π* nature. Recognising that the different models investigated all possess an electron-deficient core with electron-rich substituents, the hypothesis was made that the highest transition observed in their UV-Vis spectra was due to an intramolecular CT phenomenon. Evidence supporting such a hypothesis was found in the great sensitivity of the λ_{max} of absorption of the transition to the nature of the solvent, and more precisely its dielectric constant. In the case of **3c**, the λ_{max} is shifted from 379 nm in hexane to 397 nm in chloroform. Such a red shift with an increase of the polarity of the solvent is typical of CT transitions, since CT states are better stabilized by polar solvents.[32] As can be seen in the inset of Fig. 3, only two solvents do not follow the general trend of the increase of the λ_{max} with increasing dielectric constants: toluene and chloroform. For these two solvents additional stabilisation is believed to shift the λ_{max} further to the red. In the case of toluene, π interactions will help to stabilise the CT state, while in the case of chloroform, it is the presence of the relatively acidic protons of this solvent that leads to this phenomenon. Similar trends were observed for the different models in tetrahydrofuran, chloroform and toluene (see Supporting Information, Fig. S2†).

It will be noted that the extinction coefficient of the long wavelength CT transition does not seem to be altered anomalously by varying the concentration, or when in the solid state, which does not favour an aggregation hypothesis. Finally, the position of the λ_{max} of absorption of this band seems to be correlated to the ionisation potential of the aromatic substituents in the 2- and 6-positions (Table 2), although no linear fit could be obtained. This is further evidence of the CT nature of the transition.[32]

The second and third bands that appear in the UV-Vis spectra of models **3a–e** were assigned as the first and second

Table 2 Photophysical properties of compounds **3a–e**

Compound	IP (eV)[a]	Chloroform λ_{max}[d] (nm)	Chloroform Φ[b] (10^{-2})	Chloroform Stokes' shift (nm)	Tetrahydrofuran λ_{max}[d] (nm)	Tetrahydrofuran Φ[b] (10^{-2})	Tetrahydrofuran Stokes' shift (nm)	Toluene λ_{max}[d] (nm)	Toluene Φ[b] (10^{-2})	Toluene Stokes' shift (nm)
3a	9.24	355	Na[c]	Na[c]	343	Na[c]	Na[c]	353	Na[c]	Na[c]
3b	8.86	384	3.4	159	377	2.9	154	383	0.19	120
3c	8.63[e]	398	6.7	183	385	6.8	156	389	0.68	110
3d	8.50[f]	396	4.8	155	387	4.1	157	392	0.70	125
3e	8.89	397	6.8	145	387	4.0	165	390	0.83	127

[a] IP values obtained from the literature[33] for the corresponding unsubstituted aryl groups. [b] Fluorescence quantum yield. [c] Compound **3a** did not show any detectable fluorescence. [d] The λ_{max} of absorption of the CT band. [e] IP value found for fluorene. [f] IP value found for 3-methylthiophene.

π–π*, with a benzenoid and a quinonoid character, respectively, by analogy with the spectrum of anthraquinone (**1**). Both these bands are red shifted, compared with the first and second π–π* transitions in **1**, which is consistent with the increased conjugation in each half-molecule.

Fluorescence spectroscopy

Anthraquinone derivatives are usually considered as poorly fluorescent materials. This is due to the presence in their energy pattern of a relatively low-lying n–π* state that can act as a trap, through intersystem crossing, and shortcut radiative fluorescent decays.[32] Compound **1** itself displays no fluorescence in solution.[29] A few anthraquinone derivatives, however, display fluorescence with quantum yields reaching up to 10^{-2} in order of magnitude.[29,34,35] This is especially the case for amino and hydroxyl substituted anthraquinones. A CT phenomenon is considered to be responsible for this behaviour. However, in these cases the photophysical processes were found to be rather complex due to the presence of intra- and inter-molecular hydrogen bonding.[29,34–36]

Compounds **3b–e** were found to display relatively strong fluorescence, with solution quantum yields up to 6.8×10^{-2} (see Table 2). A typical fluorescence spectrum, for model **3e** in chloroform, is displayed in Fig. 4. The appearance of fluorescence in these 2,6-diarylanthraquinones is thought to be due to the presence of a CT state sufficiently lower than the n–π* state. Model **3a** did not display any detectable fluorescence, which is thought to be due to the fact that, for this compound, the CT state is still higher or too close to the n–π* state. The observation of CT-induced fluorescence is consistent with what was reported for amino- and hydroxyl-substituted anthraquinones and the quantum yield measured for models **3b–e** are comparable to what can be found in the literature for these derivatives.[29] Furthermore, the Stokes' shifts measured in chloroform, tetrahydrofuran and toluene are rather large (110 nm to 186 nm), which is typical of CT phenomena. However, the fluorescence quantum yields of models **3b–e** dropped by one order of magnitude when measured in toluene (Table 2). This phenomenon has still not been fully rationalized, but could indicate that the CT state is not stabilized in the same way in this solvent.

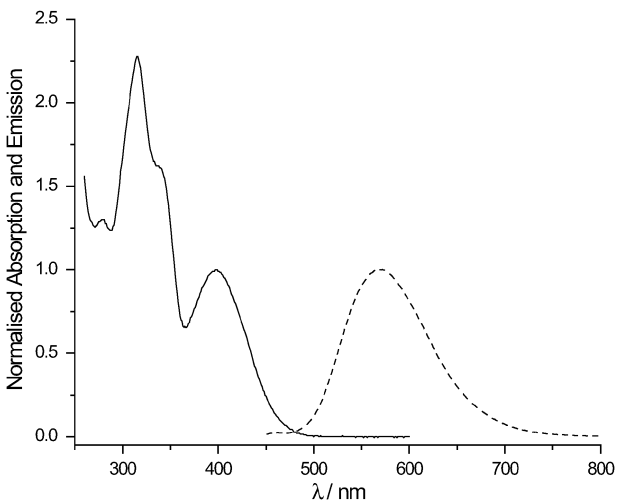

Fig. 4 UV-Vis (solid line) and fluorescence (dashed line) spectra of 2,6-bisdioctylfluorene-9,10-anthraquinone **3c** in chloroform; $\lambda_{excitation}$: 405 nm.

Here a simple parallel can be drawn with 2,7-diarylfluorenone and various fluorenone-containing polyfluorenes which show comparable long wavelength fluorescence.[37–39] Two different scenarios have been presented to account for such long wavelength fluorescence. First, fluorenone is known to undergo excimer formation upon visible light excitation and such species may then emit light at longer wavelength.[37] Second, a CT phenomenon occurs between the electron-rich aromatic substituents and the fluorenone moiety.[38,39] In each case, evidence has been presented to support or to rule out both hypotheses. Given the structural analogy of anthraquinone and fluorenone derivatives, as well as their similar energy patterns, our results tend to favour the latter scenario.

Cyclic voltammetry

A large amount of research and numerous articles have been devoted to the study of electrochemical processes in quinones.[40–43] This obviously reflects their applications and importance in the field of chemistry and biology. Cyclic voltammograms of anthraquinone (**1**) are known to display two successive reduction peaks, corresponding to two successive one-electron transfers. The first reduced state generated, the semiquinone state, is a radical state and the second reduced state is a dianion (depending on the experimental conditions). A numerical model was developed by Zuman and co-workers to predict the position of the first reduction peak of various quinones, including anthraquinone derivatives.[40,44] This model is based on the Hammett theory and can be described by eqn (1), where ρ and σ_p are the Hammett reaction and substituent constants, respectively and H is the Hammett term

(which is equal to $\Delta E_{1/2}$, the difference between the half-wave potentials of 1 and the compound of interest, in the absence of additional effects). Zuman found that for anthraquinone derivatives, σ_p gave better agreement with experimental measurements than other substituent constants such as σ_m.[40,44]

$$\Delta E_{1/2} = \rho \times \Sigma\sigma_p = H \quad (1)$$

Models **3a–e** display similar voltammograms, although varying in shape and position of the peaks. A typical example is given in Fig. 5 (others can be found in the Supporting Information, Fig. S3†). In the cases of **3b** and **3d**, we did not observe any evidence of electropolymerisation, as could have been expected. In order to compare the results of the different models and anthraquinone (**1**), the voltammograms were recorded in anhydrous, degassed dichloromethane. The positions of the peaks are reported in Table 3. Unfortunately, the σ_p values for the different aromatic substituents are not available in the literature, so no quantitative predictions can be made. However, σ_p can qualitatively be expected to be negative for electron-rich aromatic substituents and the overall effect is to shift the first half-wave potential to more negative values. As can be seen in Table 3, this is not the case. This phenomenon can be rationalised by introducing another term in eqn (1), arising from aromatic destabilisation. Let us call this term *P*. Now eqn (1) rewrites into (2).

$$\Delta E_{1/2} = \rho \times \Sigma\sigma_p + P = H + P \quad (2)$$

The aromatic destabilisation term *P* arises from the destabilization of the aromatic ring as described previously in this article. Its effect is to lower the energy barrier to the transition state, since the aromatic character of the aromatic ring is lowered. *P* is thus expected to be positive and to shift the first reduction half-wave potential to more positive values. A similar effect has previously been reported by Buschel and co-workers[45] and, more recently, by Gouloumis *et al.* in phthalocyanine-anthraquinone conjugates.[46] For models **3a–e**, aromatic destabilisation occurs, giving rise to a high positive *P* term in eqn (2), which counterbalances the negative *H* term. The overall effect of these two phenomena (the electrostatic Hammett effect and the aromatic destabilisation) is to shift the first reduction half-wave potential to more positive values. However, no correlation could be observed between the ionisation potential of the aromatic substituent and the position of the first reduction half-wave potential (Table 3). This seems to indicate that the magnitudes of both *H* and *P* terms do not follow the same trends. However, since no data are available on the σ_p values for the different aromatic substituents used, no further conclusions could yet be drawn from these results. Comparison of the first reduction potential of the different derivatives with that of a standard such as ferrocene[18,47] allows approximation of the EA of these compounds near 3.6 eV.

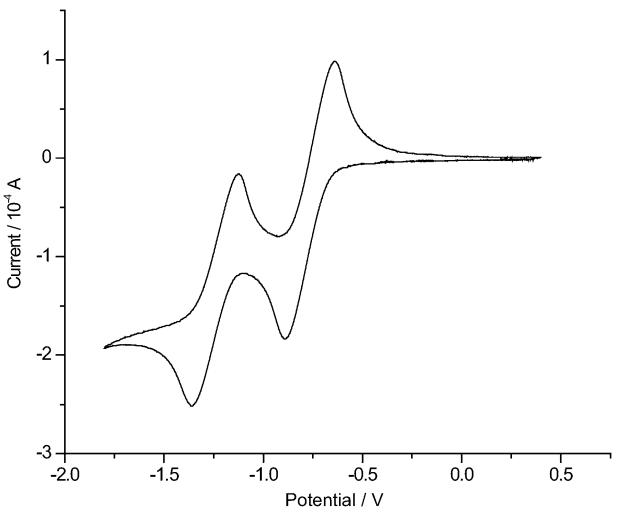

Fig. 5 CV of compound **3b** (3 mmol L^{-1}) in tetra-*n*-butylammonium tetrafluoroborate ($TBAPF_6$) (0.1 mol L^{-1}) solution in degassed anhydrous dichloromethane (scan rate: 0.1 V s^{-1}), *vs.* Ag/AgCl.

Table 3 Electrochemical properties of compounds **1** and **3a–e**[a]

Compound	$E_{1/2}$[b] (mV)	ΔE[b] (mV)	$1/2(E_{pa} + E_{pc})$[c] (mV)	ΔE[c] (mV)
1	−880	300	−1450	300
3a	−860	200	−1280	260
3b	−770	250	−1240	240
3c	−790	300	−1370	300
3d	−830	140	−1280	180
3e	−850	90	−1230	130

[a] Experiment carried out in degassed anhydrous dichloromethane solutions (electrolyte: $TBAPF_6$, 0.1 mol L^{-1}; scan rate: 0.1 V s^{-1}), *vs.* Ag/AgCl. [b] First reduction potential. [c] Second reduction potential.

Chemical doping experiments

In order to probe the nature of the negatively charged states generated upon reduction, chemical doping experiments were conducted on anthraquinone (**1**) and models **3b** and **3c**. The experiment simply consisted in reducing the desired compound, using a sodium hydrosulfite basic solution, in NMP and recording the changes in the UV-Vis spectra (Fig. 6). For all three compounds, the UV-Vis spectra recorded were very similar and displayed two strong transitions above 370 nm, near 405 and 502 nm. These two transitions were assigned by Carsky and coworkers,[48] in the case of **1**, as π–π* bands. These results are consistent with results obtained for **1** in different solvents[45,48,49] or for 2-methyl-9,10-anthraquinone in NMP and suggest the formation of dianion, fully reduced, species.

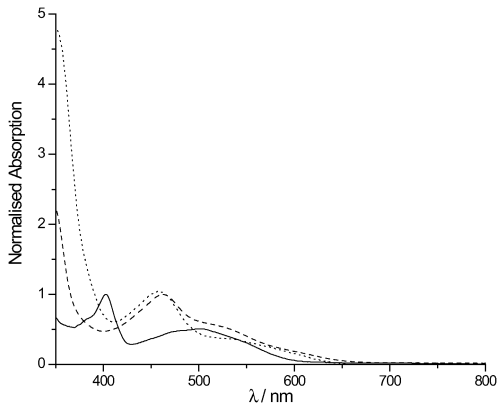

Fig. 6 Chemical doping of 9,10-anthraquinone **1** (solid line) and compounds **3b** (dashed line) and **3c** (dotted line) in NMP, using alkali solutions of sodium hydrosulfite as reducing agent.

No semiquinone form could be observed, presumably due to the low stability of this type of compounds which are prone to disproportionation.[20,48,49] The UV-Vis spectra of the reduced models **3b** and **3c** show two transitions that can be compared to the two transitions obtained for **1**. The two transitions are red-shifted in both cases, compared to **1**, although this shift remains relatively small (less than 50 nm). These results suggest that the substituents have an effect on the delocalisation of the negative charges generated upon reduction of 2,6-diaryl-9,10-anthraquinones (at least in the case of electron-rich substituents) and that the reduced systems generated are more conjugated than **1**.

Conclusions

In summary, this preliminary study has shown that many 2,6-diaryl-9,10-anthraquinones are easily accessible from the bis-triflate **2** of 2,6-dihydroxy-9,10-anthraquinone. A strong CT phenomenon is observed in these compounds, in the case of sufficiently electron-donating substituents, and is responsible for their higher fluorescence quantum yields in the yellow-orange region. The first reduction potentials of the different derivatives synthesised were shifted to more positive potentials, compared to 9,10-anthraquinone, which can be tailored by the occurrence of an aromatic destabilisation effect. EAs near 3.6 eV were measured for all of these compounds. 9,10-Anthraquinone derivatives bearing electron-rich aromatic rings in the 2- and 6-positions are therefore potentially interesting candidates for application in electronic devices such as OLEDs, OFETs, photovoltaic cells and electrochromic sensors where high electron-affinity compounds are required. However, more complete studies, especially the investigation of their solid state properties, are still required to fully conclude on this subject. Finally, the fact that the quinone moiety blocks conjugation between the two aromatic substituents in the neutral state but allows it in both reduced states could open new research avenues in molecular electronics, where an anthraquinone moiety may act as an electrochemical switch.

Acknowledgements

We would like to thank Avecia Ltd and the EPSRC (Grant No. GR/S02297/01) for financial support.

References

1 A. Kraft, A. C. Grimsdale and A. B. Holmes, *Angew. Chem., Int. Ed.*, 1998, **37**, 402.
2 R. H. Friend, E. W. Gymer and A. B. Holmes, *Nature*, 1999, **397**, 121.
3 L. Rothberg, *Nature*, 1990, **347**, 518.
4 C. D. Dimitrakopoulos and D. J. Mascaro, *IBM J. Res. Dev.*, 2001, **45**, 11.
5 H. Sirringhaus, R. J. Wilson, R. H. Friend, M. Inbasekaran, W. Wu, W. P. Woo, M. Grell and D. D. C. Bradley, *Appl. Phys. Lett.*, 2000, **77**, 406.
6 R. N. Marks, J. J. M. Halls, D. D. C. Bradley, R. H. Friend and A. B. Holmes, *J. Phys.: Condens. Matter*, 1994, **6**, 1379.
7 K. Dore, S. Dubus, H.-A. Ho, I. Levesque, M. Brunette, G. Corbeil, M. Boissinot, G. Boivin, M. G. Bergeron, D. Boudreau and M. Leclerc, *J. Am. Chem. Soc.*, 2004, **126**, 4240.
8 A. A. Argun, P.-H. Aubert, B. C. Thompson, I. Schwendeman, C. L. Gaupp, J. Hwang, N. J. Pinto, D. B. Tanner, A. G. Mac Diarmid and J. R. Reynolds, *Chem. Mater.*, 2004, **16**, 4401.
9 A. R. Brown, D. M. de Leeuw, E. J. Lous and E. E. Havinga, *Synth. Met.*, 1994, **66**, 257.
10 A. Facchetti, M.-F. Yoon, C. L. Stern, H. E. Katz and T. J. Marks, *Angew. Chem., Int. Ed.*, 2003, **42**, 3900.
11 Y. Sakamoto, T. Suzuki, M. Kobayashi, Y. Gao, Y. Fukai, Y. Inoue, F. Sato and S. Tokito, *J. Am. Chem. Soc.*, 2004, **126**, 8138.
12 J. M. Hancock, A. P. Gifford, Y. Zhu, Y. Lou and S. A. Jenekhe, *Chem. Mater.*, 2006, **18**, 4924.
13 H. E. Katz, J. L. Johnson, A. J. Lovinger and W. Li, *J. Am. Chem. Soc.*, 2000, **122**, 7787.
14 X. L. Chen and S. A. Jenekhe, *Macromolecules*, 1997, **30**, 1728.
15 C. J. Tonzola, M. M. Alam, B. A. Bean and S. A. Jenekhe, *Macromolecules*, 2004, **37**, 3554.
16 A. P. Kulkarni, Y. Zhu and S. A. Jenekhe, *Macromolecules*, 2005, **38**, 1553.
17 T. Yamamoto, M. Arai and H. Kokubo, *Macromolecules*, 2003, **36**, 7986.
18 S. Janietz, J. Barche, A. Wedel and D. Sainova, *Macromol. Chem. Phys.*, 2004, **205**, 187.
19 D. M. de Leeuw, M. M. J. Simenon, A. R. Brown and R. E. F. Einerhand, *Synth. Met.*, 1997, **87**, 53.
20 G. L. Zubay, *Biochemistry*, Wm. C. Brown, Dubuque, IA, 4th edn, 1998, ch. 17.
21 T. Yamamoto and H. Etori, *Macromolecules*, 1995, **28**, 3371.
22 Y. Muramatsu, T. Yamamoto, M. Hasegawa, T. Yagi and H. Koinuma, *Polymer*, 2001, **42**, 6673.
23 G. Power, P. Hodge, I. D. Clarke, M. A. Rabjohns and I. Goodbody, *Chem. Commun.*, 1998, 873.
24 J. E. Gautrot, P. Hodge, D. Cupertino and M. Helliwell, *New J. Chem.*, 2006, **30**, 1801.
25 D. R. Coulson, *Inorg. Synth.*, 1972, **8**, 121.
26 M. Belletete, S. Beaupre, J. Bouchard, P. Blondin, M. Leclerc and G. Durocher, *J. Phys. Chem.*, 2000, **104**, 9118.
27 J. N. Demas and G. A. Crosby, *J. Phys. Chem.*, 1971, **75**, 991.
28 C. Coudret and V. Mazenc, *Tetrahedron Lett.*, 1997, **38**, 5293.
29 A. Navas Diaz, *J. Photochem. Photobiol., A*, 1990, **53**, 141.
30 M. Nepras, J. Fabian and M. Titz, *Collect. Czech. Chem. Commun.*, 1981, **46**, 20.
31 R. H. Peters and H. H. Summer, *J. Chem. Soc.*, 1953, 2101.
32 N. J. Turro, *Modern Molecular Photochemistry*, Benjamin and Cummings, Menlo Park, CA, 1991, p. 76.
33 D. R. Lide, *Handbook of Chemistry and Physics*, CRC Press, 83rd edn, 2002–2003.
34 S. R. Flom and P. F. Barbara, *J. Phys. Chem.*, 1985, **89**, 4489.
35 M. H. Van Benthem and G. D. Gillispie, *J. Phys. Chem.*, 1984, **88**, 2954.
36 T. Yatsuhashi, Y. Nakajima, T. Shimada and H. Inoue, *J. Phys. Chem. A*, 1998, **102**, 3018.
37 M. Sims, D. D. C. Bradley, M. Ariu, M. Koeberg, A. Asimakis, M. Grell and D. G. Lidzey, *Adv. Funct. Mater.*, 2004, **14**, 765.
38 E. Zojer, A. Pogantsch, E. Hennebicq, D. Beljonne, J.-L. Bredas, P. Scandiucci de Freitas, U. Scherf and E. J. W. List, *J. Chem. Phys.*, 2002, **117**, 6794.
39 K. Becker, J. M. Lupton, J. Feldmann, B. S. Nehls, F. Galbrecht, D. Gao and U. Scherf, *Adv. Funct. Mater.*, 2006, **16**, 364.
40 P. Zuman, *Collect. Czech. Chem. Commun.*, 1962, **27**, 2035.
41 M. W. Lehmann and D. H. Evans, *J. Electroanal. Chem.*, 2001, **500**, 12.
42 N. Gupta and H. Linschitz, *J. Am. Chem. Soc.*, 1997, **119**, 6384.
43 J. Q. Chambers, *The Chemistry of the Quinonoid Compounds*, Wiley, Toronto, 1988, p. 719.
44 P. Zuman, *Collect. Czech. Chem. Commun.*, 1962, **27**, 648.
45 M. Buschel, C. Stadler, C. Lambert, M. Beck and J. Daub, *J. Electroanal. Chem.*, 2000, **484**, 24.
46 A. Gouloumis, D. Gonzalez-Rodriguez, P. Vazquez, T. Torres, S. Liu, L. Echegoyen, J. Ramey, G. L. Hug and D. M. Guldi, *J. Am. Chem. Soc.*, 2006, **128**, 12674.
47 S. Janietz, D. D. C. Bradley, M. Grell, C. Giebeler, M. Inbasekaran and E. P. Woo, *Appl. Phys. Lett.*, 1998, **73**, 2453.
48 P. Carsky, P. Hobza and R. Zahradnik, *Collect. Czech. Chem. Commun.*, 1971, **36**, 1291.
49 M. Fujihira and S. Hayano, *Bull. Chem. Soc. Jpn.*, 1972, **45**, 644.